Program Digest, 2019 IEEE International Ultrasonics Symposium (IUS)
Glasgow, Scotland, October 6-9, 2019

The Impact of Analog Front-end Filters on Ultrasound Harmonic Imaging

Meiyi Zhou[1], Sotir Ouzounov[2], Massimo Mischi[1], Eugenio Cantatore[1], Pieter Harpe[1], Email: m.zhou@tue.nl
[1]Department of Electrical Engineering, Eindhoven University of Technology, Eindhoven, the Netherlands
[2]Philips research, Eindhoven, the Netherlands

***Abstract*—Ultrasound (US) harmonic imaging has shown advantages in better spatial resolution and contrast compared to classic fundamental imaging, but it suffers from more attenuation due to the increased frequency. To achieve more penetration, high dynamic range (DR) front-end electronics is required to receive the weak harmonic components. Typical US front-ends use a variable gain amplifier (VGA) to compensate part of the required DR, in order to avoid using a highly sensitive analog-to-digital converter (ADC). However, in harmonic imaging, the received signal amplitude is dominated by the fundamental component, thus the VGA is less efficient for these small harmonics. An analog front-end filter can be used before the VGA to mitigate this issue but this has an impact on spatial resolution by changing the dominant frequency component and spatial pulse length of the received signal. In this work, a combined acoustic-and-electronic model is made to understand the impact of the use of an analog front-end filter in US harmonic imaging applications in terms of imaging resolution, contrast, and hardware requirements.**

Keywords— ultrasound harmonic imaging, spatial resolution, contrast, front-end electronics, analog filter

I. Introduction

US harmonic imaging is routinely used in clinical ultrasound diagnosis [1], [2]. In this method, low-frequency fundamental waves are transmitted, while multiples of the fundamental frequency (n = 2, 3, …) produced by non-linear propagation are received. The harmonic components are isolated from the fundamental to generate the images. This approach shows improvements in image quality, i.e. better spatial resolution and contrast-to-noise ratio (CNR) [3], [4]. Several digital imaging processing techniques, such as harmonic band filtering and phase cancellation [5] are widely used to screen out the fundamental. However, for both cases, the signal-to-noise ratio (SNR) and the imaging depth are easily limited by the DR of front-end electronics, since the harmonics are much weaker than the fundamental. Therefore, improving the DR of front-end electronics is important for US harmonic imaging.

Conventionally, to achieve a high DR, most commercial or published US imaging systems [6], [7] use the receiving path shown in Fig. 1. It contains a low noise amplifier (LNA), a VGA for time gain compensation (TGC), and an ADC. Both the LNA and the VGA can compensate for the reduced penetration [7], thus the total DR of the receiving path is increased without the need for a highly sensitive ADC. This architecture works well for fundamental imaging but is not ideal for harmonic imaging. In harmonic imaging, since the power of the target harmonic component is much lower than the power of the fundamental, the use of a VGA is less effective. As shown in Fig. 2 (a), the fundamental component is dominant in the received signal, thus

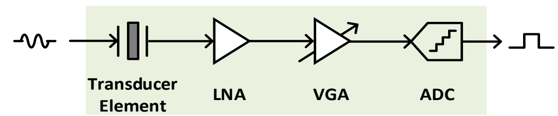

Fig. 1. Illustration of a conventional US receiving path.

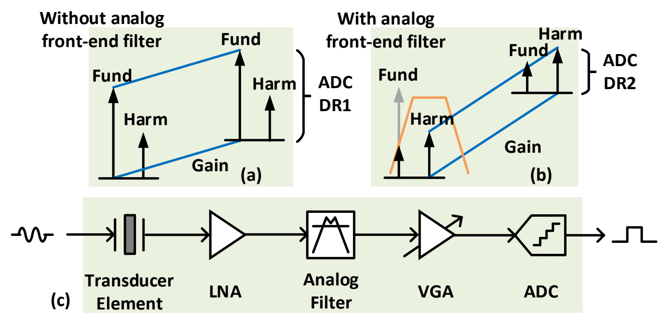

Fig. 2. Illustration of the DR compensation scheme without (a) and with (b) an analog front-end filter, and (c) ultrasound receiving path with an analog filter before the VGA.

limiting the amplification of the weak harmonic components, and thus requiring a high-DR ADC. Considering this, introducing a harmonic band filter before the VGA in the analog hardware domain can mitigate this issue (Fig. 2 (b) and (c)): the strong fundamental component is attenuated before amplification, such that a higher gain can be applied to the weak harmonics, leading to a relaxed DR for the ADC. Since the harmonics are relatively far away from the fundamental in the spectrum, a low-order analog front-end filter can already provide significant suppression of the undesired fundamental component. Compared to a digital post-filter used in signal processing, the analog filter can either relax the ADC's DR, or produce better SNR. As a penalty, the received bandwidth is irreversibly reduced after filtering, which may have an impact on both the lateral resolution (LR) and axial resolution (AR). Therefore, understanding the trade-offs between analog filtering, imaging performance, and hardware requirements, helps to optimize US harmonic imaging systems. To the best of our knowledge, this is not yet studied in the literature.

In this paper, the impact of analog filtering is studied in a combined acoustic-and-electronic simulation model for US harmonic imaging. The ultrasound simulator K-Wave [8] is used to generate the time domain non-linear acoustic wave fields, then a model of the electronic front-end is built to further process and filter the received echo signals, and finally the image is reconstructed. Our target is to demonstrate how the introduced analog filtering influences the imaging quality as well as the front-end electronics design. The obtained results are presented and discussed in the following sections.

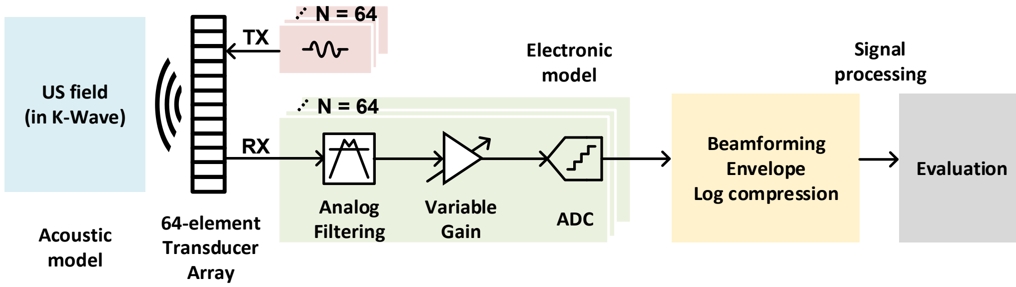

Fig. 3. Overview of the ultrasound system modeled in MATLAB.

II. Methods

Fig. 3 shows the combined acoustic-and-electronic model, that is integrated in MATLAB. The ultrasound simulator K-Wave is used to generate acoustic data for ultrasound harmonic imaging. This is next processed by a model of the electronics and followed by image reconstruction algorithms. Without loss of generality, for the example studied in this paper, the transducer is modeled as a 64-element linear array and centered on the origin of the US field. The frequency response of the transducer is defined by a Gaussian filter with a center frequency of 6 MHz and a -3 dB bandwidth of 100 % for both transmitting and receiving. Each transducer element has a pitch size of 100 µm (kerf = 0). The transducer array is set to perform 60 scan lines, covering a planar sector from $-\pi/3$ to $\pi/3$ rad. The transmit focusing depth is 15 mm for each scan. To implement harmonic imaging, the transducer is excited by two-cycle sinusoids at 3 MHz (f_0 = 3 MHz).

A two-dimensional (2D) imaging medium is modeled in K-Wave with a spatial resolution of 50 µm. The sampling frequency used for simulations is 100 MHz. For modeling power law absorption, the attenuation coefficient is 0.54 dB/MHz/cm and the power law exponent is set to 1.5. The parameter of nonlinearity (B/A = 8) is also applied in the US field [8]. Two different phantoms are modeled and simulated in K-Wave: a point phantom to analyze spatial resolution, and a cyst to analyze CNR. The point phantom is created by placing a scatter point at the transmit focal depth in a homogeneous medium with a sound speed of 1540 m/s (C_0) and a medium density of 1000 kg/m^3 (ρ_0). The point target is given a 10% difference in speed of sound and medium density from the surrounding to generate an appreciable reflection. A hyperechoic cyst phantom is also created. It is located at the transmit focal depth with a radius of 1 mm. The contrast is generated from acoustic reflections by modulating the sound speed and density at each grid point [8]. The cyst is generated by defining a circular heterogeneous region with randomly Gaussian distributed scatters with 10% variation of C_0 and ρ_0. The surrounding background is composed of randomly Gaussian distributed scatters with a lower variation of C_0 and ρ_0 (0.5%).

The received echo signals from the US field are first filtered by the transducer as mentioned previously, converting the acoustic signals to electric signals. The receiving path model includes three main blocks: an analog filter, a VGA and an ADC. The analog filter is implemented by a Butterworth bandpass filter with tunable filter order and bandwidth. The filter has a center frequency at the third harmonic (9 MHz) relative to the fundamental frequency. The VGA is assumed to be able to perform any gain factor with infinite bandwidth. The ADC has a Nyquist bandwidth of 50 MHz. The maximum signal amplitude that the ADC can convert is aligned with the maximum output signal from the transducer. For simplification, other non-idealities of the electronics, i.e. mismatch and distortion, are not simulated in this work, thus the received harmonic components are only generated by the US field. The quantized signals are further processed with standard beamforming, Hilbert envelope detection, and log compression to reconstruct the image.

III. Results and Discussion

In this section, the simulation results based on the two described phantoms are presented. The point target simulation shows the impact of the filter order and bandwidth to spatial resolution with ideal electronic performance. The cyst phantom shows the benefit of the analog filter with limited electronic performance.

A. Point target simulation

The point phantom is simulated to demonstrate the impact of an analog front-end filter on the spatial resolution. The spatial resolution can be divided into axial and lateral resolutions. The lateral resolution (LR) of a focused beam is determined by the following factors [9]:

$$LR \propto \frac{Focal\ depth\ \times wavelength}{Aperture\ size} \tag{1}$$

The axial resolution (AR) depends on the spatial pulse length [9], shown in the following equation:

$$AR \propto \frac{Spatial\ pulse\ length}{2} \tag{2}$$

With fixed transducer and focal depth, the analog front-end filter influences the wavelength in (1) by changing the dominant frequency component, and the spatial pulse length in (2) by reducing the bandwidth simultaneously.

To show the effect of the analog filter, both VGA and ADC are ideal and the receiving path is thermal-noise free. Fig. 4 (a) shows the B-mode images from the point scatter. The left image is acquired by the raw data from the transducer, which shows the original spatial resolution. The axial resolution is much better than the lateral resolution thanks to the short transmit pulses. In the right image of Fig. 4 (a), the received echo signals are processed with a 2nd order bandpass filter with 2 MHz bandwidth. As expected, *LR* is improved after filtering since *LR* is proportional to the wavelength. However, *AR* is degraded, since the spatial pulse length increases with reduced bandwidth,

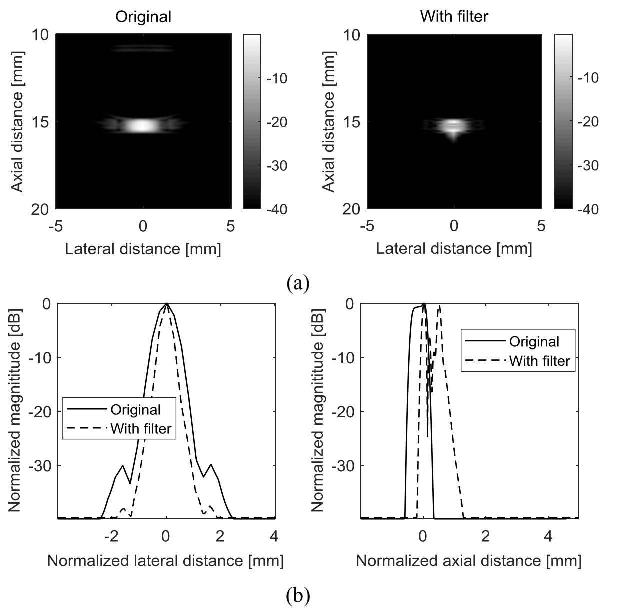

Fig. 4. (a) B-mode imaging of point phantom (DR = 40 dB); (b) Normalized lateral and axial cross-sections of the B-mode images from (a).

TABLE I. COMPARISON OF PERFORMANCE

	Original (m)	With filter (n)	Difference (n/m-1)
LR [mm]	**1.78**	**1.22**	**- 31.5%**
AR [mm]	**0.75**	**0.98**	**+ 30.7%**

thus a trailing region is introduced after filtering. These effects can be quantitatively shown by plotting the normalized central lines in both lateral and axial directions as shown in Fig. 4 (b). To compare the resolution difference, the full width at half maximum dynamic range (FWHMDR) [10] is used as metric. Compared to the commonly used full width at half maximum (FWHM) metric, the FWHMDR is more effective to compare the resolution achieved by a complicated US imaging system [10]. As shown in Table I, the *LR* shows 31.5% improvement and the *AR* is degraded by 30.7% after filtering. Since the overall spatial resolution of a US system is determined by max(*LR*, *AR*), the overall spatial resolution of this US system still improves by 31.5%.

To fully understand the impact of the filter order and bandwidth on spatial resolution, similar simulations are made with filter order from 1st to 3rd and bandwidth from 1 MHz to 4 MHz, while the center frequency remains the same at the 3rd harmonic (9 MHz). As shown in Fig. 5, the lateral resolution is more sensitive to the filter order than the bandwidth. For the axial resolution, the 1st order filter shows negligible impact over the full bandwidth. However, both the 2nd and the 3rd order filter will degrade the axial resolution considerably. The impact is the most pronounced when the filter bandwidth is low. The results also show that filters with different order and bandwidth can balance between *LR* and *AR*, and in this way the overall spatial resolution can be maximized. For example, a 2nd or 3rd order filter with appropriate bandwidth selection can balance *LR* and *AR*. While the proposed filter can be applied either in the analog or digital domain, an analog filter has the additional advantage of relaxing the requirements for the front-end electronics, which will be discussed later.

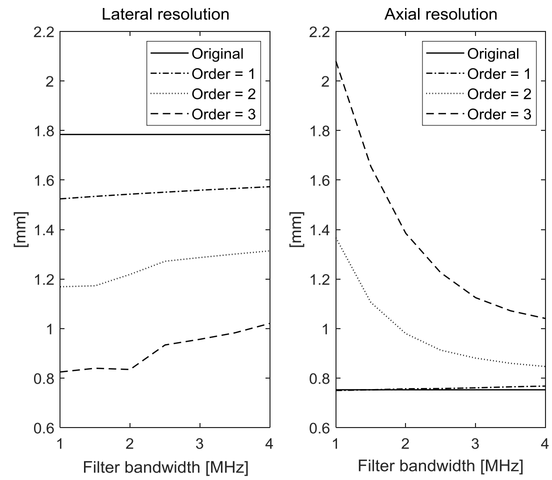

Fig. 5. Lateral and axial resolution with different filter order (from 1st to 3rd order) and different bandwidth (from 1 to 4 MHz per 0.5 MHz step).

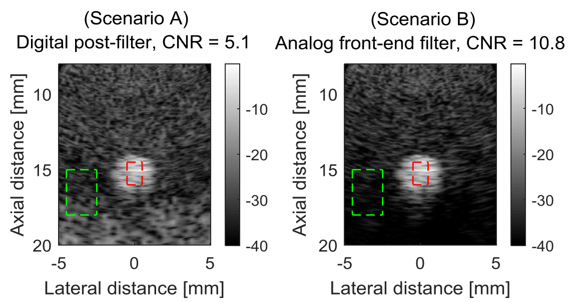

Fig. 6. B-mode images of the cyst phantom with digital post-filter (left) and analog front-end filter (right).

B. *Cyst phantom simulation*

The previous simulations show the filter impact with ideal front-end electronics on spatial resolution. Here, the imaging performance of the entire US system is assessed by means of CNR. A cyst phantom is simulated with diffused scatters as described in Section II. In this simulation, both the VGA and the ADC are included to demonstrate the effect of the front-end electronics. Thermal noise of the hardware is also included in this case, which is set to a level of -65 dB with respect to the maximum signal amplitude at the transducer.

The absolute requirements of the VGA gain and the ADC resolution are related to the definition of the scatters in the cyst and the background. Therefore, comparisons are made between two scenarios. In scenario A, the received signals are processed by the conventional US receiving path (only VGA and ADC) and then filtered by a digital post-filter. In scenario B, the signal is first processed by the analog front-end filter, then amplified by the VGA to the maximum level that the ADC can support, and then quantized by the ADC. In both cases, a second-order band-pass filter with a bandwidth of 1.5 MHz is chosen based on the results in Section II. Because the analog filter can suppress the fundamental component in the received signals, the VGA in scenario B can provide 40 dB more gain to amplify the filtered signals as shown in Fig. 2.

Fig. 6 shows the images of the two scenarios when the ADC resolution is 7 bit. To quantify the differences, the CNR for each of the images is calculated. CNR is defined as the difference between the mean of the background (μ_b) and the cyst (μ_s) in

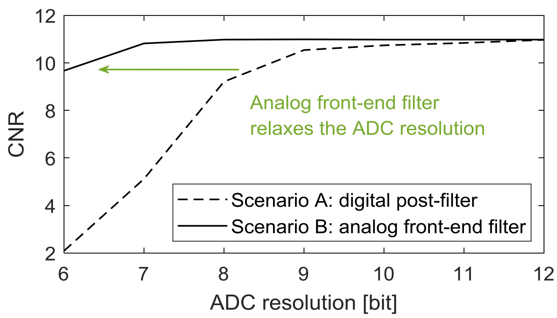

Fig. 7. CNR vs ADC resolution.

dB divided by the standard deviation of the background (σ_b) in dB [11]. Regions used to define CNR are shown in the red and green rectangles for the cyst and background, respectively. The images are shown with 40-dB dynamic range. As shown in Fig. 6, the CNR of the right image (10.8) is improved substantially compared to the left (5.1). More noise and clutter are observed in the left image. This is because in scenario A the ADC resolution is insufficient to convert the weak harmonic components, resulting in low SNR. In scenario B, thanks to the analog filter, higher VGA gain is possible, such that the same ADC can now digitize the harmonics with a higher SNR. Similar simulations are made with ADC resolutions varying from 5 bit to 12 bit. The results in Fig. 7 demonstrate the analog filter's ability to relax the ADC resolution in the front-end design for harmonic imaging. In this case, the original ADC requirement is about 9 to 10 bit to avoid CNR loss, while after applying the analog front-end filter before the ADC, this is relaxed by 3~4 bit.

Although we have demonstrated the ability to relax the ADC resolution requirements, in practice, the reduction is dependent on the difference in signal strength between the fundamental and harmonic. For example, with a transmit frequency of 3 MHz, the two-way attenuation of the fundamental in a 6-cm scan is 19 dB. For the 2^{nd}, 3^{rd} and 4^{th} harmonic, the attenuation is increased to 29 dB, 39 dB and 49 dB, which means the harmonics can be 10 dB, 20 dB, and 30 dB lower than the fundamental only due to the absorption. Therefore, the reduction in the ADC resolution is more evident when receiving higher-order harmonics with the same filter order and bandwidth. Reduction in ADC resolution is very beneficial for ADC design in terms of power consumption, chip area, and design complexity. For example, designing an ADC with 4 bit less resolution saves 16x-256x power if the same Walden/Schreier figure-of-merit is achieved [12]. On the other hand, the time step for receive beamforming is supposed to be higher for harmonic imaging. Therefore, the sampling speed of the ADC should also be increased, normally exceeding 50 MHz, if high harmonics (3^{rd}, 4^{th}, 5^{th} …) are of interest. Considering this high sampling speed, reducing ADC resolution is also helpful for reducing the output data rate of an array-based US system with many converters. As a cost, a band-pass filtering stage should be implemented before the VGA stage in hardware.

IV. Conclusion

In this work, combined acoustic-and-electronic simulations are performed to clarify the impact of an analog filter on 3^{rd} harmonic imaging. Both point phantoms and cyst phantoms are simulated based on B-mode imaging. The results show a trade-off between spatial resolution, CNR, and front-end design complexity. The lateral resolution is less affected by the filter bandwidth but benefits from increasing filter order. The axial resolution is less influenced by 1^{st} order filtering, while remarkably degraded by 2^{nd} and 3^{rd} order filtering when narrow filter bandwidth is used. The results also demonstrate that moderate filtering can achieve a balance between lateral resolution and axial resolution, and overall lead to better spatial resolution. The use of an analog filter also improves CNR with the help of a VGA. Compared to a digital post-filter used after the ADC, an analog front-end filter relaxes the requirements of the ADC resolution by several bits, especially in harmonic imaging. Overall, analog filtering in the front-end is foreseen to enhance the image quality of US harmonic imaging systems while reducing ADC hardware requirements.

Acknowledgment

This work is part of the research programme Locate with project number 15282, which is financed by the Netherlands Organisation for Scientific Research (NWO). The authors would like to thank Prof. dr. ir. J.M.J. den Toonder for technical discussion.

References

[1] F. Tranquart, N. Grenier, V. Eder and L. Pourcelot, "Clinical use of ultrasound tissue harmonic imaging", Ultrasound in Medicine & Biology, vol. 25, no. 6, pp. 889-894, 1999.

[2] F. Duck, "Nonlinear acoustics in diagnostic ultrasound", Ultrasound in Medicine & Biology, vol. 28, no. 1, pp. 1-18, 2002.

[3] B. Ward, A. Baker and V. Humphrey, "Nonlinear propagation applied to the improvement of resolution in diagnostic medical ultrasound", The Journal of the Acoustical Society of America, vol. 101, no. 1, pp. 143-154, 1997.

[4] R. Lencioni, D. Cioni and C. Bartolozzi, "Tissue harmonic and contrast-specific imaging: back to gray scale in ultrasound", European Radiology, vol. 12, no. 1, pp. 151-165, 2001.

[5] T. Desser and R. Jeffrey, "Tissue harmonic imaging techniques: Physical principles and clinical applications", Seminars in Ultrasound, CT and MRI, vol. 22, no. 1, pp. 1-10, 2001.

[6] M. Chen et al., "A Pixel Pitch-Matched Ultrasound Receiver for 3-D Photoacoustic Imaging With Integrated Delta-Sigma Beamformer in 28-nm UTBB FD-SOI", IEEE Journal of Solid-State Circuits, pp. 1-14, 2017.

[7] H. Attarzadeh, Y. Xu and T. Ytterdal, "A Low-Power High-Dynamic-Range Receiver System for In-Probe 3-D Ultrasonic Imaging", IEEE Transactions on Biomedical Circuits and Systems, vol. 11, no. 5, pp. 1053-1064, 2017.

[8] B. Treeby, J. Jaros, A. Rendell and B. Cox, "Modeling nonlinear ultrasound propagation in heterogeneous media with power law absorption using a k-space pseudospectral method", The Journal of the Acoustical Society of America, vol. 131, no. 6, pp. 4324-4336, 2012.

[9] A. Ng and J.Swanevelder, "Resolution in ultrasound imaging", Continuing Edu. Anaesthesia, Crit. Care Pain, pp. 186-192, 2011

[10] S. Harput, J. Mclaughlan, D. M. J. Cowell, and S. Freear, "New performance metrics for ultrasound pulse compression systems," 2014 IEEE International Ultrasonics Symposium, 2014.

[11] S. Krishnan, K. Rigby, and M. Odonnell, "Improved estimation of phase aberration profiles," IEEE Transactions on Ultrasonics, Ferroelectrics and Frequency Control, vol. 44, no. 3, pp. 701–713, 1997.

[12] B. Murmann, "ADC Performance Survey 1997-2018," [Online]. Available: http://web.stanford.edu/~murmann/adcsurvey.html.